The Role of Water Coordination in Binary Mixtures. A Study of Two Model Amphiphilic Molecules in Aqueous Solutions by Molecular Dynamics and NMR

R. Sinibaldi,[†] C. Casieri,[‡] S. Melchionna,[†] G. Onori,[§] A. L. Segre,[||] S. Viel,[||] L. Mannina,[||,⊥] and F. De Luca*[,†]

SOFT-INFM-CNR Research Center and Dipartimento di Fisica, Università La Sapienza, I-00185 Roma, Italy, SOFT-INFM-CNR Research Center and Dipartimento di Fisica, Università dell'Aquila, I-67010 L'Aquila, Italy, SOFT-INFM-CNR and Dipartimento di Fisica, Università di Perugia, CEMIN (Centro di Eccellenza Materiali Innovativi Nanostrutturati) I-06100 Perugia, Italy, Istituto di Metodologie Chimiche, CNR Area della Ricerca di Roma, I-00016 Monterotondo Stazione (Rome), Italy, and Dipartimento di S.T.A.A.M., Università degli Studi del Molise, I-86100 Campobasso, Italy

Received: November 28, 2005; In Final Form: February 13, 2006

Two binary aqueous mixtures which contain the small amphiphilic molecules TMAO (trimethylamine-*N*-oxide) and TBA (*tert*-butyl alcohol) have been investigated by molecular dynamics simulations and NMR chemical shift and self-diffusion measurements. TMAO is an osmolyte, while TBA is a monohydrate alcohol. Both possess bulky hydrophobic groups and polar heads, namely, NO in TMAO and OH in TBA. The hydrophilic/hydrophobic content of these isosteric molecules strongly modulates the structure and dynamics of the hydration shell, which is thought to be responsible for the effects observed on proteins and phospholipids. Simulation results, especially on hydrogen-bond networking, spatial correlations, and self-diffusivity, are consistent with NMR data and agree well with previous numerical studies on similar solutions. The methods employed allow the elucidation of the microscopic features of the solutions. For TBA solutions, the hydration shell is found to have a low density and a large spatial spread, and thus, above the molar fraction of 0.03, reduction of hydrophobic hydration drives self-aggregation of the solute. This effect does not take place in TMAO solutions, where the hydration shell is more compact and stable, maintaining its structure over a wider range of solute concentrations.

I. Introduction

TMAO (trimethylamine-*N*-oxide) and TBA (*tert*-butyl alcohol) are small amphiphilic molecules with similar structures (Figure 1). They are characterized by bulky hydrophobic moieties formed by a tertiary butyl or trimethylammonium and by hydrophilic parts characterized by different electrostatic dipole moments. TBA is a water-soluble alcohol, while TMAO is water-soluble only below a critical concentration value. The dipole moment of TMAO is about 5 D, i.e., three times larger than that of TBA.

The differences in dipole moments, hydrogen-bond propensity, and hydrophobic−hydrophilic content could be reasons for the different action exerted by TBA and TMAO on biological systems. TBA promotes protein denaturation, while TMAO neutralizes the destabilizing effect of urea on proteins and increases their stability.[1−3] TMAO is found in organisms living in conditions of stress, such as high salinity, high temperature, and high pressure.[4] Literature data agree on the fact that both TBA and TMAO are excluded from the protein domains.[5,6] The indication that the action of TBA and TMAO on proteins occurs through a strong perturbation of the solvent properties is supported by computational[1] and experimental data on nucleic acids and proteins[7,8] and on the micellization of several surfactants.[9] Moreover, the behavior of TBA and TMAO aqueous solutions resembles many biological systems, where apparently similar molecules have different effects on aqueous solutions.

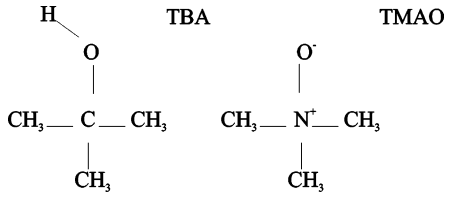

Figure 1. Schematic view of the TBA and TMAO molecules.

The main goal of the present paper is to fully characterize the hydration features of TBA and TMAO. The comparison between these two bulky molecules allows the analysis of the details of the solute−water interaction at finite concentration and, thus, the identification of the interactions exerted by the amphiphilic traits in modulating water coordination. This study may shed some light on the general role of hydration in driving self-aggregation of amphiphilic molecules.

We have studied the hydration mechanism of aqueous solutions of TBA and TMAO in the water-rich region. Our study has been performed by NMR measurements of ^{13}C and ^{1}H chemical shifts and self-diffusion coefficients and by molecular dynamics (MD) simulations.

The MD results on diffusivity can be directly compared with the experimental self-diffusion coefficients, whereas a com-

* To whom correspondence should be addressed. E-mail: francesco.deluca@roma1.infn.it.
[†] Università La Sapienza.
[‡] Università dell'Aquila.
[§] Università di Perugia.
[||] CNR Area della Ricerca di Roma.
[⊥] Università degli Studi del Molise.

10.1021/jp056897+ CCC: $33.50
Published on Web 04/11/2006

parison with chemical-shift data can be done only indirectly. Actually, NMR chemical shifts can only be accessed by electronic structure calculations, not via the classical force field in our MD simulations. Nevertheless, MD provides detailed information at the atomistic level, including hydrogen-bond statistics and radial distribution functions, that can be employed to qualitatively interpret chemical-shift data.

Several physical properties of TBA aqueous solutions, such as the adiabatic compressibility,[10] the C−H stretching frequencies,[11] and the apparent molar volume,[9,12] exhibit some anomalies in the structure and dynamics of solutions at a molar fraction of about 0.025, suggesting a possible clustering of the solute molecules. No anomaly of this type appears in TMAO solutions where the solute−solute direct interactions seem to be completely absent.[9,13] To the best of our knowledge, several articles report NMR studies on TBA solutions,[14−17] while NMR data on TMAO aqueous solutions are not found in the literature.

Some theoretical and computational studies appear in the past on these molecules. Yoshida et al.[18] used integral equation theory to calculate the radial distribution function for molar fraction larger than 0.1 and found qualitative agreement with neutron scattering measurements,[19] providing evidence for solute self-assembly. Previous MD investigations on TBA aqueous solutions mainly concerned the hydrophobic hydration process, indicating TBA clustering at high molar fractions.[20,19] Some MD studies focused on the interplay between TMAO and water coordination.[1,21] Actually, only a few MD investigations[22,23] were devoted to a comparative analysis of TBA and TMAO aqueous solutions and included comparison with experimental data.[9,11,13,24] In ref 22, MD was used to investigate single molecules of TBA and TMAO in water. TMAO resulted in a smaller hydration volume than TBA, while coordinating water molecules more tightly than TBA. In a subsequent study,[23] the same authors investigated the properties of both solutions versus concentration. Strong differences in hydration of the two solutes were found. In particular, the hydration number of TBA was found to decrease above a threshold concentration, while TMAO hydration remained almost constant in the investigated concentration range.

The paper is organized as follows. In section II, experimental and computational methods are described. In section III, NMR and MD data are reported and discussed in two separate parts, the first one related to self-diffusion, hydration, and hydrogen-bond statistics, and the second one related to chemical-shift results and aggregation features. Concluding remarks are made in section IV.

II. Materials and Methods

A. Sample Preparation and Viscometer. TBA and TMAO solutions were studied in the water-rich region $0 < X_2 < 0.1$, where the solute molar ratio is defined as $X_2 = n_{sol}/(n_{sol} + n_{water})$.

TBA (Sigma Aldrich) and TMAO (Sigma Aldrich) were dissolved into bidistilled water from which dust particles were removed with micrometer filters. Binary solutions were prepared using a balance with an accuracy of 0.1 mg to weight a minimal quantity of 40 mg in the most dilute solutions of TBA and TMAO. All measurements were carried out at 298 K immediately after sample preparation in order to avoid preferential evaporation and therefore composition changes. Solutions were kept in a temperature bath for at least 15 min before any measurement were performed; the temperature of the thermal bath was monitored continuously with a precision digital thermometer, which varied less than ±0.05 K during each measurement.

Kinematic viscosities were measured with a factory-calibrated Cannon Ubbelhode suspended-level viscometer. Flow times were measured with a stop watch, and measurements were repeated until the relative error was smaller than 1%. Typically, flow times were longer than 600 s; therefore, the relative uncertainties of measured flow times due to systematic errors are expected to be negligible. Flow time values of the mixtures were converted to relative viscosity

$$\eta_{rel} = \frac{\rho_1 t_1}{\rho_0 t_0} \tag{1}$$

where ρ_1 refers to the density of the mixtures, ρ_0 is the density of pure solvent, and t_1 and t_0 are the measured values of mixture and water flow times, respectively. A kinematic energy correction was considered to be unnecessary on account of long flow times in the experimental setup.

Density values (data not shown) were measured with an Anton Paar model DMA and agree with previous published data.[9,12]

B. NMR. All NMR experiments were performed at 298 K on a Bruker Avance AQS600 spectrometer operating at 600.13 MHz with a multinuclear inverse z-gradient probehead. ^{1}H and ^{13}C chemical shifts (δ scale) were determined from simple pulse-and-acquire spectra and were referenced with respect to $CHCl_3$. Specifically, the spectra were recorded once with a number of scans optimized to yield an acceptable signal-to-noise ratio. Then, a capillary tube containing $CHCl_3$ was inserted into the sample tube, and the spectra were recorded again with a reduced number of scans. No correction for magnetic susceptibility effects was applied. The gradient coil of the probehead was calibrated by using the diffusion coefficient of deuterated water (HOD) at 298 K (1.9010^{-9} m^2 s^{-1}).[25,26] In this way, a value of 55 G cm^{-1} for the gradient coil constant was obtained. The reliability of the gradient calibration for more slowly diffusing compounds was further checked by measuring the diffusion coefficient of octanol; the obtained diffusion coefficient value, 1.410^{-10} m^2 s^{-1}, agreed well with published data.[27]

The self-diffusion coefficients of TBA and TMAO were monitored by pulsed-field gradient (PFG) NMR experiments. The stimulated echo sequence incorporating bipolar gradient pulses and a longitudinal eddy current delay (BPP-LED) was used.[28] In the BPP-LED experiment, the amplitude of an NMR signal observed at the echo is given by the expression[29]

$$I = I_0 \exp\left[-D(\gamma g \delta)^2\left(\Delta - \frac{\delta}{3} - \frac{\tau}{2}\right)\right] \tag{2}$$

where I_0 is the resonance amplitude at zero gradient strength; γ is the magnetogyric ratio of the proton; g, δ, and Δ are the strength, the duration, and the separation of the gradient pulses, respectively; and τ is the gradient pulse recovery time. The gradient strength was logarithmically incremented in 16 steps from 2% up to 95% of the maximum gradient strength. Diffusion times and gradient pulse durations were optimized for each experiment to achieve a 95% decrease in the resonance intensity at the largest gradient amplitude; typically, diffusion times between 100 and 500 ms and bipolar sine gradient pulses of 1.4 ms were employed. The longitudinal eddy current delay was held constant at 25 ms, whereas the gradient pulse recovery time was set to 0.1 ms. After Fourier transformation and phase correction, the baseline of the spectra was carefully adjusted. The data were analyzed by plotting the signal intensities (areas) as a function of the gradient strength and fitting the resulting decay curves to eq 2 with a nonlinear least-squares fit (Simplex

algorithm) by using the relaxation module of the Bruker *Xwinnmr* software package (version 3.5). All data were well-described by a single exponential.[16]

C. Computational Details. Simulations were performed at eleven different concentrations, namely, in pure water conditions and for TBA and TMAO solutions at $X_2 = 0.01$, 0.02, 0.03, 0.05, and 0.08. Temperature was always fixed to $T = 298$ K. At all concentrations, the number of solute molecules was set to 125, so that the number of water molecules was varied to obtain the desired concentration, resulting in 12 375 water molecules for the most diluted solutions. The chosen number of solute molecules is large enough to observe any aggregation trend in the low concentration range under study and to collect sufficient statistics for further analysis.

Both solutes and water were modeled by an all-atom-based potential energy function, taking into account bonding and nonbonding terms

$$U(\{r\}) = \frac{1}{2}\sum_{\text{angle}} K_\theta(\theta - \theta_0)^2 + \frac{1}{2}\sum_{\text{dihedrals}} K_\chi[1 + \cos(n\chi - \delta)] + \sum_i\sum_{j\neq i}\left\{4\epsilon_{ij}\left[\left(\frac{\sigma_{ij}}{r_{ij}}\right)^{12} - \left(\frac{\sigma_{ij}}{r_{ij}}\right)^{6}\right] + \frac{q_i q_j}{4\pi\epsilon_0 r_{ij}}\right\} \quad (3)$$

where $\{r\}$ represents the set of N atomic coordinates, K_θ, K_χ are angular and dihedral force constants, θ_0 is the equilibrium values for bond angles, and n and δ represent dihedral angles multiplicity and phase. Nonbonding parameters consist of Lennard-Jones and Coulomb interactions. Bonding and nonbonding parameters were taken from ref 20 for TBA and from ref 30 for TMAO. Cross-species Lennard-Jones parameters were handled via the Lorentz−Berthelot combination rule

$$\sigma_{\alpha\beta} = \frac{(\sigma_{\alpha\alpha} + \sigma_{\beta\beta})}{2} \quad (4)$$

$$\epsilon_{\alpha\beta} = (\epsilon_{\alpha\alpha}\epsilon_{\beta\beta})^{1/2} \quad (5)$$

Water was modeled by the three sites point charge model known as TIP3P.[31] The water model is consistent with the chosen force field for the solutes, and we did not attempt to employ a different one. However, a more refined water model could be invoked in subsequent studies. All chemical bonds were constrained to a fixed distance by use of the Shake algorithm.[32] Periodic boundary conditions were invoked in all simulations, which were performed with a cubic simulation cell. Accordingly, nonbonded short-range interactions were truncated beyond a cutoff of 9 Å (minimum image convention), while electrostatic interactions were treated by means of the Ewald summation method.[33] The equations of motion were integrated in time by using the velocity Verlet algorithm[34] with a time step of 1 fs.

Solutions were initially generated by placing the center of mass of each solute molecule onto a cubic lattice with spacing of 7 Å and surrounded by the appropriate number of water molecules. To initially equilibrate the system, 80-ps-long simulations were run for all systems under study. At this stage, the solutions were left to approach equilibrium in the isobaric−isothermal (NPT) ensemble by allowing the internal pressure to relax to 1 atm while the system volume rearranged accordingly. The NPT dynamics was implemented by means of the Nosè−Hoover equations of motion[34] with a piston time constant of 2 ps and a thermostat time constant of 0.5 ps. A representative configuration extracted over the last 25 ps of equilibration was chosen as the starting configuration for the subsequent production runs. The starting configuration was such that its volume was the closest to the volume averaged over the final 5 ps of equilibration. Subsequently, each system was run for 200 ps in the canonical (NVT) ensemble. A Nosè−Hoover thermostat was used to control temperature[35] with a thermostat time constant of 0.5 ps. For most situations, the Nosè−Hoover thermostat does not affect the transport coefficients appreciably, while a constant-pressure dynamics may induce artifacts on the transport coefficients. For this reason, we chose a constant-pressure simulation only for the equilibration stage. One configuration every 25 fs was stored for further analysis.

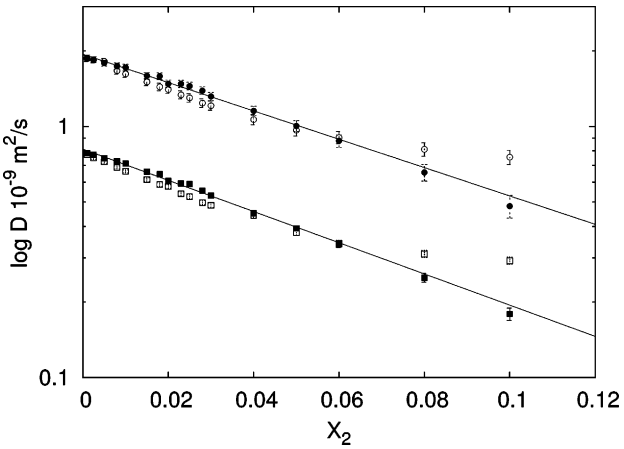

Figure 2. Diffusion coefficient obtained from NMR data vs molar fraction: Open circles refer to water in TBA solution; open squares refer to TBA. Filled circles refer to water in TMAO solution and filled squares to TMAO.

The large number of solute molecules allowed us to perform relatively short runs to obtain accurate averages on diffusivity and distribution functions. The diffusion coefficient was computed via the Einstein relation

$$\lim_{t\to\infty}\frac{1}{N}\sum_i^N\langle|\, r_i(t) - r_i(0)|^2\rangle = 6Dt \quad (6)$$

The diffusion coefficient D was determined in the time window $0.6 < t < 1.5$ ns, an interval large enough to be in the linear regime and short enough to avoid re-entrant acoustic waves arising from periodic boundary conditions. The diffusion coefficient was computed for the oxygen atom of water, the central carbon atom of TBA, and the nitrogen atom of TMAO.

III. NMR and Molecular Dynamics Results

The NMR and MD data will be next reported in two separate sections, the first one concerning self-diffusion and hydration data, and the second one concerning chemical-shift results.

A. Self-Diffusion and Hydration Statistics. The NMR−PFG data on self-diffusion (Figure 2) show a continuous decreasing of water and solute mobility with increasing TBA or TMAO concentrations: Both water and solute diffusivities decrease by about four times in the interval $0 < X_2 < 0.1$. Data reported in logarithmic scale show a linear decrease in the TMAO solution, while in the TBA solution, there is a net change in the slope of self-diffusion at $X_2 \simeq 0.05$ (Figure 2) for both solute and solvent. This is also apparent in the MD results (Figure 3). At low solute concentrations, water and TMAO diffuse slightly more rapidly than water and TBA in TBA solutions, while above $X_2 \simeq 0.05$, water and TBA in TBA solutions diffuse more rapidly than

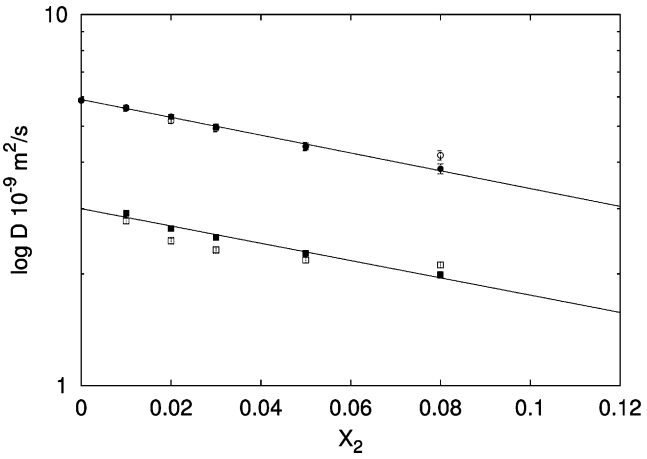

Figure 3. Diffusion coefficient vs molar fraction obtained from MD data. Symbols are the same as Figure 2.

TABLE 1: Frequency of Occurrence of 1, ..., 5 H-bonds between Water Molecules (f_1, ..., f_5)[a]

X_2	f_1	f_2	f_3	f_4	f_5	$\bar{n}$
			TMAO			
0%	0.022	0.139	0.372	0.400	0.063	3.32
1%	0.023	0.143	0.381	0.391	0.059	3.30
2%	0.023	0.144	0.387	0.389	0.056	3.26
3%	0.023	0.145	0.393	0.384	0.054	3.22
5%	0.023	0.147	0.402	0.371	0.053	3.13
8%	0.024	0.153	0.423	0.350	0.047	3.00
			TBA			
1%	0.023	0.143	0.377	0.394	0.059	3.30
2%	0.023	0.142	0.378	0.396	0.058	3.28
3%	0.023	0.145	0.380	0.394	0.056	3.25
5%	0.024	0.149	0.385	0.388	0.052	3.18
8%	0.027	0.161	0.393	0.373	0.044	3.06

[a] $\bar{n}$ represents the mean number of H-bonds per single water molecule. Data are obtained by excluding solute−solvent counts from the analysis.

water and TMAO in TMAO solutions. This behavior is confirmed also by MD data on self-diffusion, as presented in Figure 3.

The qualitative agreement between the NMR and MD results is quite satisfactory. However, the quantitative differences can be traced back to the water model employed, which provides diffusion coefficients different from the experimental values by a factor of 2.3.[36] In fact, different water models used in previous MD studies on TBA solutions[20,37] (specifically MCY and SPCE water models) showed a water diffusion coefficient closer to our NMR results than to our MD results using the TIP3P water model. The results reported in Figures 2 and 3 differ from those reported by Noto et al.[22] who studied single-molecule solutions, which had a faster diffusivity of water in TBA than in TMAO solutions. We notice that both NMR-DOSY and MD data show water diffusivity with the same qualitative decay with concentration for both solutes (Figures 2, 3), suggesting that the interaction between solute and water plays a significant role in self-diffusion.

A regular decrease of diffusivity of water is fully observable in Figures 2 and 3. The NMR and MD data for $X_2 < 0.05$ may be explained by the simple picture based on a regular increase of water molecules involved in the hydration of TBA and TMAO with concentration. In this view, the diffusivity of solute and solvent is reduced by the steric hindrance exerted by the bulky molecules on self- and cross-diffusion. Moreover, a solvent-mediated mechanism can reduce the diffusivity of both the solute and the solvent. In fact, the self-diffusion coefficient of solutes decreases with X_2 because more tightly bound water molecules imply a higher diffusional barrier for the solutes. However, some differences exist between the diffusive behavior of TBA and TMAO solutions. Both NMR-DOSY data and MD results agree with the fact that in the $0 < X_2 < 0.05$ interval the self-diffusion coefficient reduces more in TBA than in TMAO solutions. This minor difference between the self-diffusion coefficients may be ascribed to the different hydration attitudes of TBA and TMAO. The spatial organization of water around the two solutes is illustrated by the solute−solvent radial distribution functions (Figure 4a,b) showing that the hydration shell of TMAO is formed by a larger number of water molecules and is closer to the solute than that of TBA.[9,23] Above $X_2 \simeq 0.05$, water and TBA diffuse more rapidly than in the case of TMAO solutions, as also confirmed by MD (Figure 2), signaling a structural rearrangement of the solute.

In Table 1, we report the mean number of water−water H-bonds $\bar{n}$ at different concentrations.[38] In both TMAO and TBA solutions, $\bar{n}$ decreases very slightly as X_2 increases, while the mean number of hydrogen bonds (HB) decreases with X_2 whether the average number of HB per water molecule is counted considering water−solute bonds or not (Table1), in agreement with neutron scattering data.[39]

The data in Table 1 indicate that the probability that one water molecule is involved in a large number of hydrogen bonds is slightly higher for TBA than for TMAO. Data in the literature agree with the fact that, in TBA solutions, hydrophobic hydration is reduced above $X_2 = 0.02-0.03$,[23] where direct TBA−TBA contacts screen the methyl groups from the solvent, and as a result, water experiences a stronger coordination with itself. This is further demonstrated in Figure 5 where the water−water radial distribution function for the two mixtures is reported. The solute−water radial distribution function (Figure 4a−d) shows that water molecules are localized closer to the solute in TMAO rather than in TBA solutions. It is thus plausible that, in the presence of TMAO, water experiences a steric hindrance which reduces the probability to form a substantial number of HBs. The mean HB number between solute and water does not change with concentration, the values being 2.5 HB for TMAO, 1.3 for TBA as acceptor, and 0.8 for TBA as donor.

Relevant information about interfacial water can be extracted by studying the population of hydration water around each solute. The number of water molecules contained in a shell of thickness $\delta = 3$ Å, around each solute molecule α, can be computed by

$$N_\alpha = \sum_{i \in \text{water}} \theta(r_{i\alpha} - \delta) \qquad (7)$$

where θ is the characteristic function and $r_{i\alpha}$ the minimum distance between each solute atom and water oxygen atom. In a recent paper,[24] the mean hydration number values of both solutes were extrapolated from IR data showing that the hydration number of TMAO slightly decreased with concentration, while for TBA a strong decrease with increasing concentration was observed.

Therefore, we analyzed the fluctuations of the hydration number, defined as the number of oxygen atoms located at distance $\delta < 3$ Å from a solute atom belonging to a methyl groups. The observed values strongly confirm that the TBA hydration shell around a nonpolar atom is softer than that around TMAO, with the former having higher fluctuations than the latter (Figure 6). Interestingly, hydration remains constant for TMAO, while for TBA, it increases slightly up to $X_2 \simeq 0.03$

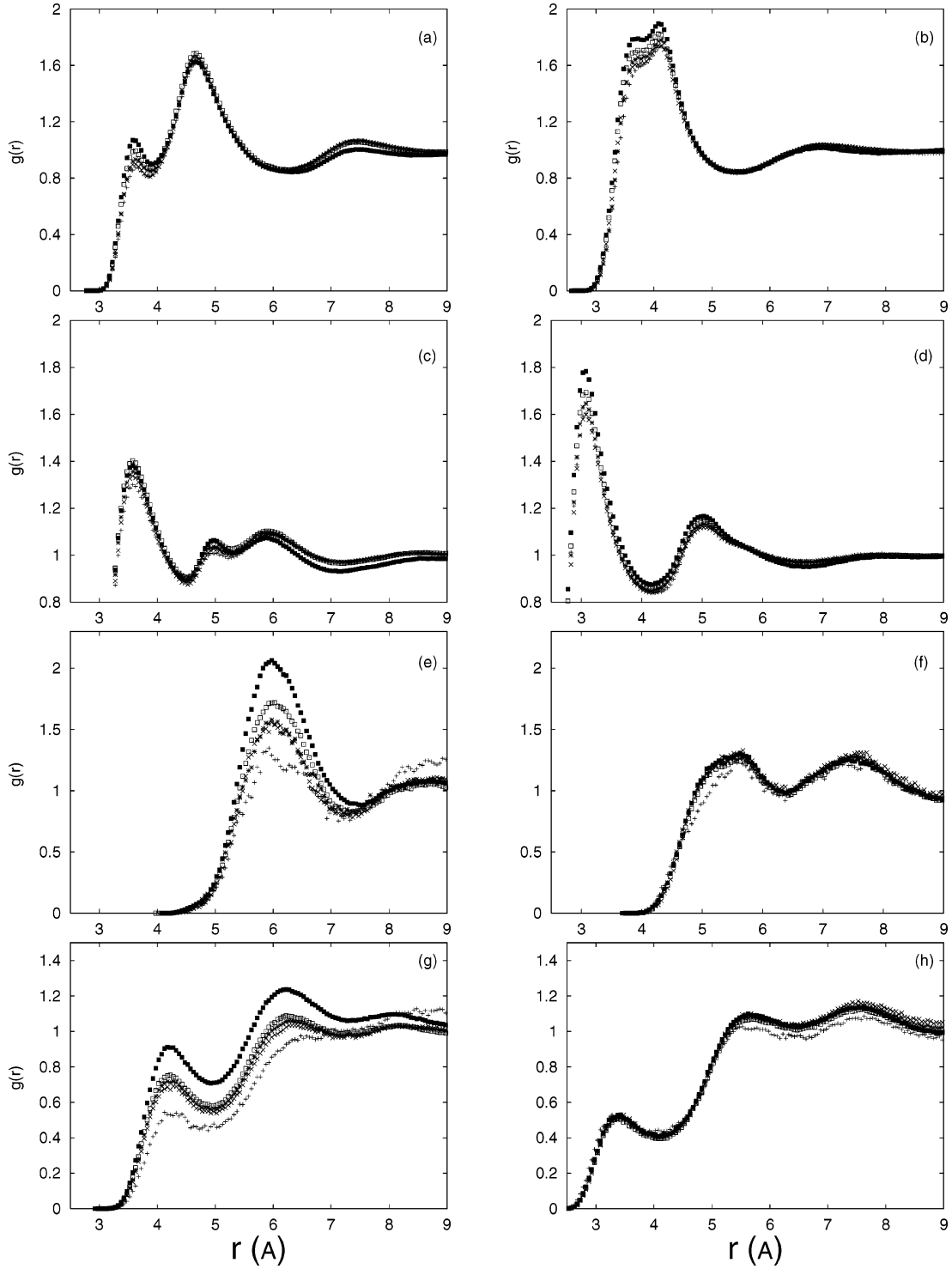

Figure 4. Solute−solute and solute−water radial distribution functions, for TBA solutions (left panel) and for TMAO solutions (right panel): (a) C_c-O_w, (b) $N-O_w$, (c,d) C_m-O_w, (e) C_c-C_c, (f) N−N, (g,h) C_m-C_m. Symbols refer to different concentration: (+) $X_2 = 0.01$; (×) $X_2 = 0.02$; (∗) $X_2 = 0.03$; (□) $X_2 = 0.05$; (■) $X_2 = 0.08$.

and then decreases. The peak in the fluctuations could be due to the formation of unstable solute−solute aggregates of different size.

For $X_2 > 0.03$, the average number of water molecules coordinated to TBA is reduced,[24,23] and thus, the water in the TBA solution has a lower density[9] and a lower viscosity (Figure 7) with respect to the water in the TMAO solution; as a result, in TBA solutions, water is softer than in TMAO solutions and therefore offers a lower diffusional barrier to the solute.

A further verification of the above conclusions comes from studying the radial distribution function of water−methyl groups, as reported in Figure 4c,d. The plots show that the average distance of water oxygen from the carbon of the methyl groups is larger for TBA than for TMAO. The average number of water molecules coordinated by one molecule of TBA does not change appreciably between $X_2 = 0.05$ and $X_2 = 0.08$, while it increases almost regularly in TMAO solutions. Differences in the aggregation behavior of the two solutes are also evidenced by the radial distribution function of the central atoms in TBA (C_c-C_c) and in TMAO (N−N) solutions (Figure 4e,f). The N−N profile of the TMAO solutions does not change with X_2 and exhibits two characteristic peaks indicating a certain degree of

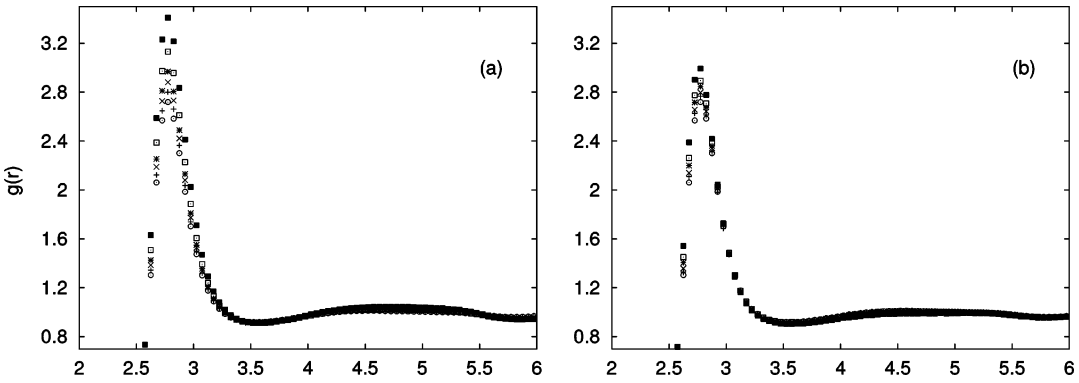

Figure 5. Water−water radial distribution functions centered on oxygen atoms. Left panel refers to TBA solution, right panel to TMAO. Symbols are the same as Figure 4. Moreover, open circles refers to pure water condition.

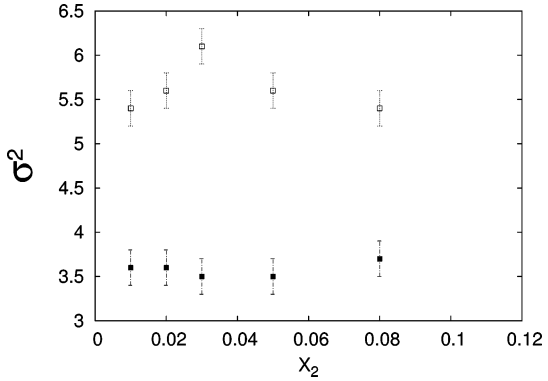

Figure 6. Fluctuations in the number of water molecules surrounding the hydrophobic region of the solutes vs molar fraction (see text for details). Open squares refer to TBA, filled squares to TMAO.

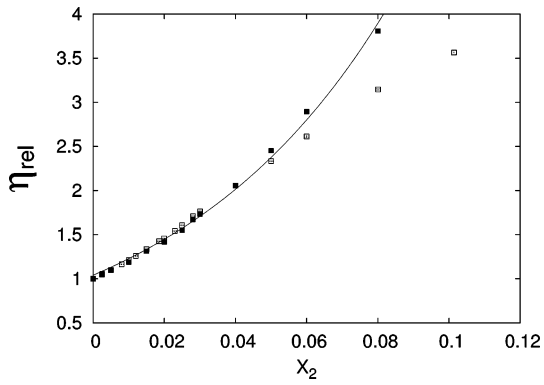

Figure 7. Relative viscosity η. Open squares refer to TBA, filled squares to TMAO.

order in the location of the molecules. In the TBA solutions, a clear increase of C_c-C_c correlation is seen above $X_2 \leq 0.02$, in full agreement with IR data and previous MD simulations.[11,20,23] Incomplete mixing at the molecular level and water segregation were found in water−alcohol mixtures at high concentrations of methanol and ethanol, where polar heads were found to point toward each other, explaining well-known anomalous thermodynamic data.[15,40,41]

In the TBA−water system, the situation appears to be different. At high X_2, the hydrophobic parts of TBA are essentially surrounded by other alcohol molecules, leaving the TBA−water interface nearly unchanged as the concentration increases. On the other hand, an extended intermixing of TMAO molecules and water persists up to the highest concentration investigated.

B. Chemical Shift. The increase of NMR chemical shift (CS) with respect to a reference value generally means that protons

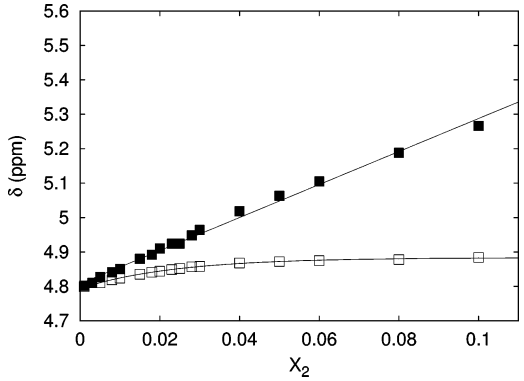

Figure 8. ^{1}H CS variation of water vs solute concentration: Open squares refer to TBA, filled squares to TMAO.

experience an electron deshielding effect, namely, a local decrease of the electronic density of the molecular bond. This might occur, for example, when two molecular groups approach each other more closely than the sum of their van der Waals radii. Chemical exchange of nuclei between two different chemical sites, with different CS, can modify the NMR spectrum. When the jumping frequency between the two sites is greater than the separation between their CS (fast exchange), the result is a single line, which depends on the relative spin populations of the two sites. In the slow exchange limit, two CSs result, in addition to some line-shape broadening.

For $X_2 < 0.03$, the hydrogen exchange between coordinated and bulk water is in the fast regime, as indicated by the single ^{1}H−CS line that is observed in the NMR spectra. The ^{1}H−CS of water in the TMAO solutions increases almost linearly vs X_2, while that of TBA solutions becomes approximately constant above $X_2 \simeq 0.03$ (Figure 8). The linear increase of CS for $X_2 < 0.03$ in both solutions is consistent with the fast exchange regime picture, the variation of the ^{1}H−CS being determined only by the relative population of the two waters. Such an increase is particularly marked for TMAO. This aspect independently confirms the stronger polarization of water in the presence of TMAO than in the presence of TBA, supporting the notion that water molecules are more tightly coordinated by TMAO than by TBA. Above $X_2 \leq 0.03$, the ^{1}H−CS of water of TMAO solutions keeps increasing almost linearly (Figure 8). On the other hand, for TBA solutions, the same ^{1}H−CS is nearly constant (Figure 8), as expected because of the reduction of hydration water once TBA starts clustering; this feature agrees with the faster diffusivity of water in TBA solutions than in TMAO solutions (Figure 2) and the larger fluctuations of water molecules coordinated to TBA (Figure 6). The fast exchange regime delimits the experimental information obtainable from

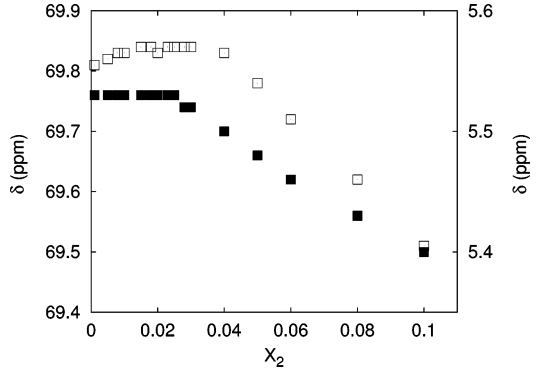

Figure 9. CS variation of ^{1}H in the hydroxyl of TBA (right axis, open squares) and of ^{13}C (left axis, filled squares).

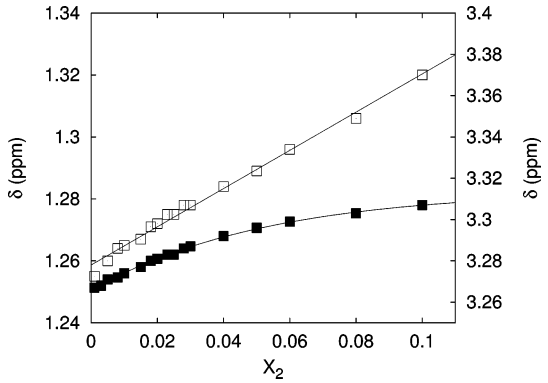

Figure 10. ^{1}H CS variation of the hydrogen atoms belonging to the methyl group: Open squares refer to TBA (left axis), filled squares refer to TMAO (right axis).

^{1}H−CS essentially to what concerns the relative dynamics of populations of the two ^{1}H−CS sites. It is thus extremely difficult to single out the electronic behavior of the hydrogen bonds versus X_2 due to the mixing of the two spin populations and the sign of the ^{1}H−CS shift, which cannot be resolved anymore.

In our NMR experiment, we were able to resolve the ^{1}H−CS line of water from that of the hydroxyl group of TBA. Both the ^{1}H−CS of water and that of the hydroxyl group of TBA increase with concentration below $X_2 \leq 0.03$. The ^{1}H−CS of the hydroxyl drops linearly when concentration is raised, possibly because of an intramolecular charge rearrangement of the TBA molecule. Nevertheless, the observed decrease shows unambiguously that the hydroxyl hydrogen exchanges with water for $X_2 > 0.03$, since direct contact between two TBA hydroxyl results in higher polarization of ^{1}H−CS, as shown in previous work on monohydrate alcohols.[15]

The ^{1}H−CS of the methyl groups probe the chemical environment even without any chemical exchange. The results are reported in Figure 10. In the TMAO solutions, there is a clear, although very small, exponential increase of the ^{1}H−CS toward a plateau. As already stated, this behavior indicates a local electronic depolarization of methyl bonds caused by the repulsive interaction exerted by water over the electronic clouds of the methyl groups. In the radial distribution function, the short distance correlation between the methyl carbon of TMAO and the water oxygen increases (Figure 4d), and this agrees with the exponential increase of the ^{1}H−CS. Thus, there is increasing correlation between water and TMAO's methyl groups vs concentration, as shown in Figure 4b.

The ^{1}H−CS of the methyl groups of TBA solutions shows a similar behavior to that of TMAO solutions up to $X_2 \leq 0.03$ and increases almost linearly above this threshold. The depolarization indicates that the electronic deshielding effect on

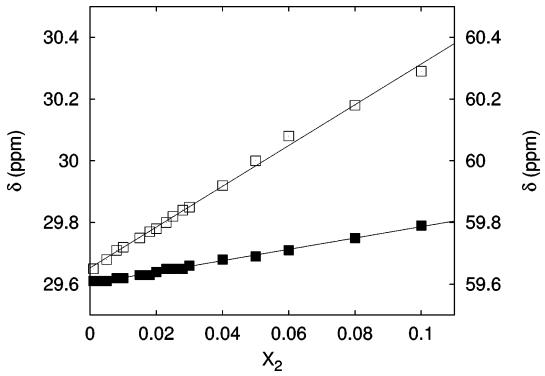

Figure 11. ^{13}C CS variation of carbon atoms belonging to the methyl group: Open squares refer to TBA (left axis), filled squares refer to TMAO (right axis).

TBA methyl groups depends on the solute concentration, further indicating that in this range of concentration clustering of TBA molecules takes place. In such aggregates, methyl groups face each other, while a repulsive methyl−methyl character slowly increases as the size of the aggregate increases. In Figure 11, the ^{13}C−CS of methyl groups are reported for both TBA and TMAO solutions. The results show that there is a very small, but significant, variation of the shielding effect on methyl carbons, clearly associated to that reported in Figure 10. Because of electroneutrality,[42] an opposite variation is expected on the central carbon of TBA. Above $X_2 \leq 0.03$, the ^{13}C−CS variation is apparent, although it is, also in this case, very small (Figure 9). These observations further confirm the repulsive interaction between the hydrogens of the methyl groups whose effects propagate on all TBA carbons. The effect increases with X_2 because of the cumulative occurrence of the interaction arising from several TBA molecules which take part in the cluster. A similar experimental observation was reported for the C−H stretching frequency of TBA,[11] as a consequence of the alteration of the electronic distribution of the C−C and C−H molecular bonds produced by TBA clustering.

Conclusion

All of the experimental and computational results presented in this paper present evidence that TMAO has a stronger hydrophilic character than TBA. In fact, at very low solute concentrations, the central difference between the two solutions resides mainly in the smaller hydration radius and the larger number of water molecules coordinated to TMAO rather than to TBA. As a result, in TMAO solutions, water packs more effectively and has a more compact hydration shell. The strong ordering action exerted by TMAO on water is ascribed to its electric dipole moment, about 5 D.[22,23] This is independently validated by analyzing the solute−solvent radial distribution function and the proton chemical shift of water. Overall, the hydration shell of TMAO proves more stable than that of TBA.

Depending on the measured quantities, the onset of clustering of TBA is found at $X_2 \leq 0.04 \pm 0.01$ and is signaled by a modification of the water−solute interface due to the reduced hydrophobic interaction. The different behavior of these two isosteric molecules is manifest, since in TMAO, the hydration shell is rather robust and prevents the solutes from clustering. On the other hand, TBA possesses a weaker hydration shell, which, above a concentration threshold, does not compensate for the thermodynamic force leading to the TBA−TBA contact.

The results of the present work have shed some light on the thermodynamic forces driving self-aggregation in simple model systems of amphiphilic molecules. Overall, we have clearly

demonstrated that the hydrophobic component of the solutes is mainly responsible for self-aggregation, despite the different polarity of the two species which, on the basis of simple electrostatic considerations, would have favored stronger aggregation of TMAO over that of TBA.

Acknowledgment. A.L.S. thanks the Società Italiana di Spettrochimica e Spettrofisica which partially supported this work.

References and Notes

(1) Zou, Q.; Bennion, B.; Daggett, V.; Murphy, K. *J. Am. Chem. Soc.* **2002**, *124*, 1192.
(2) Yancey, P. H.; Clark, M. E.; Hand, S. C.; Bowlus, R. D.; Somero, G. N. *Science* **1982**, *217*, 1214.
(3) Bennion, V. D. B. J.; DeMarco, M. L. *Biochemistry* **2004**, *43*, 12955.
(4) Trieberg, J. R.; Driedzic, W. R. *J. Exp. Zool.* **2002**, *12*, 12.
(5) Arakawa, T.; Timasheff, S. *Biophys J.* **1985**, *47*, 411.
(6) Cordone, L.; Cupane, A.; Vitrano, E. *J. Mol. Liq.* **1989**, *42*, 213.
(7) Cinelli, S.; Onori, G.; Santucci, A. *J. Phys. Chem B* **1997**, *101*, 8029.
(8) Cinelli, S.; Onori, G.; Santucci, A. *Colloid Surf.* **1999**, *160*, 3.
(9) Freda, M.; Onori, G.; Santucci, A. *Phys. Chem. Chem. Phys.* **2002**, *4*, 4979.
(10) Onori, G.; Santucci, A. *J. Mol. Liq.* **1996**, *69*, 161.
(11) Freda, M.; Onori, G.; Santucci, A. *J. Phys. Chem. B* **2001**, *105*, 12714.
(12) Kipkemboi, K.; Easteal, A. J. *Can. J. Chem.* **1994**, *72*, 1937.
(13) Freda, M.; Onori, G.; Santucci, A. *J. Mol. Struct.* **2001**, *153*, 565.
(14) Harris, K. R.; Newitt, P. J. *J. Phys. Chem. A* **1999**, *103*, 6508.
(15) Mizuno, K.; Kimura, Y.; Morichika, H.; Nishimura, Y.; Shimada, S.; Maeda, S.; Imafuji, S.; Ochi, T. *J. Mol. Liq.* **2000**, *85*, 139.
(16) Price, W. S.; Ide, H.; Arata, Y. *J. Phys. Chem. A* **2003**, *107*, 4784.
(17) Yoshida, K.; Ibuki, K.; Ueno, M. *J. Chem. Phys.* **1998**, *108*, 1360.
(18) Yoshida, K.; Yamaguchi, T.; Kovalenko, A.; Hirata, F. *J. Phys. Chem. B* **2002**, *106*, 5042.
(19) Bowron, D. T.; Finney, J. L.; Soper, A. K. *J. Phys. Chem. B* **1998**, *102*, 3551.
(20) Kusalik, P. G.; Lyuvartsev, A. P.; Bergman, D. L.; Laaksonen, A. *J. Phys. Chem. B* **2000**, *104*, 9533.
(21) Sharp, K. A.; Madan, B. *J. Chem. Phys.* **2001**, *114*, 1791.
(22) Noto, R.; Martorana, V.; Emanuele, A.; Fornili, S. L. *J. Chem. Soc., Faraday Trans.* **1995**, *91* (21), 3803.
(23) Fornili, A.; Civera, M.; Sironi, M.; Fornili, S. L. *Phys. Chem. Chem. Phys.* **2003**, *5*, 4905.
(24) Michele, A. D.; Freda, M.; Onori, G.; Santucci, A. *J. Phys. Chem.* **2004**, *108*, 6145.
(25) Price, W. S.; Stilbs, P.; Jonsson, B.; Soderman, O. *J. Magn. Reson.* **2001**, *150*, 49.
(26) Mils, R. *J. Phys. Chem.* **1973**, *77*, 685.
(27) Holz, M.; Weingartner, H. *J. Magn. Reson.* **1991**, *92*, 115.
(28) Wu, D.; Chaen, A.; C. S. J., Jr. *J. Magn. Reson.* **1995**, *115*, 260.
(29) Stejskal, E. O.; Tanner, J. E. *J. Chem. Phys.* **1965**, *42*, 288.
(30) Kast, K. M.; Brickmann, J. *J. Phys. Chem. A* **2003**, *107*, 5342.
(31) Jorgensen, W.; Chandrasekhar, J.; Madura, J.; Impey, R.; Klein, M. *J. Chem. Phys.* **1983**, *79*, 926.
(32) Ryckaert, J. P.; Ciccotti, J.; Berendsen, H. *Comput. Phys.* **1977**, *23*, 327.
(33) Allen, M.; Tildesley, D. J. *Computer Simulation of Liquids;* Clarendon: Oxford, 1987.
(34) Frenkel, D.; Smit, B. *Understanding molecular simulation: from algorithms to applications*; Academic Press: San Diego, 1996.
(35) Nosè, S. *Mol. Phys.* **1984**, *52*, 255.
(36) Jorgensen, W.; Chandresekhar, J. *J. Chem. Phys.* **1983**, *79*, 926.
(37) Tanaka, H.; Nakanishi, K.; Touhara, H. *J. Chem. Phys.* **1984**, *81*, 4065.
(38) Ferrario, M.; Haughney, M.; McDonald, I. R.; Klein, M. L. *J. Chem. Phys.* **1990**, *93*, 5156.
(39) Soper, A. K.; Finney, J. L. *Phys. Rev. Lett.* **1993**, *71*, 4346.
(40) Dixit, S.; Crain, J.; Poon, W. C. K.; Finney, J. L.; Soper, A. K. *Nature (London)* **2003**, *416*, 829.
(41) Guo, J.; Luo, Y.; Augustsson, A.; Kashtanov, S.; Rubensson, J.; Shuh, D.; Ågren, H.; Nordgren, J. *Phys. Rev. Lett.* **2003**, *91*, 157401.
(42) Capitani, D.; Rossi, E.; Segre, A. L.; Giustini, M.; Luisi, P. *Langmuir* **1993**, *9*, 685.